

Research Article

Preparation of Stellerite Loading Titanium Dioxide Photocatalyst and Its Catalytic Performance on Methyl Orange

Hua Chen,^{1,2,3} Jianhua Wang,¹ Huajun Wang,¹ Fei Yang,² Jia-nan Zhou,³ Jiajun Fu,³ Jie Yang,³ Zheng Yuan,³ and Bingbing Zheng³

¹Zhejiang Yongtai Paper Co. Ltd., Hangzhou 311421, China

²State Key Lab of Pulp and Paper Engineering, South China University of Technology, Guangzhou 510640, China

³Zhejiang Provincial Key Lab for Chem & Bio Processing Technology of Farm Product, School of Light Industry, Zhejiang University of Science and Technology, Hangzhou 310023, China

Correspondence should be addressed to Fei Yang; 7008774@qq.com

Received 7 October 2015; Accepted 11 November 2015

Academic Editor: Bao Yu Xia

Copyright © 2015 Hua Chen et al. This is an open access article distributed under the Creative Commons Attribution License, which permits unrestricted use, distribution, and reproduction in any medium, provided the original work is properly cited.

TiO₂/stellerite composite photocatalysts were prepared by dispersing TiO₂ onto the surface of HCl, NaOH, or NaCl treated stellerite using a sol-gel method. The materials were characterized by scanning electron microscopy (SEM), energy dispersive X-ray (EDX), Fourier transform infrared spectroscopy (FT-IR), BET surface area analysis, and X-ray diffraction (XRD). HCl and NaCl modification result in the promotion of the pore formation at the stellerite surfaces and induced the microscopic changes, while the surface morphology and structure of the stellerite were almost ruined by NaOH modification. Supported TiO₂ calcinated at 200°C presented anatase structure. The photocatalytic degradation activities of TiO₂ loaded HCl and NaCl modified stellerite were better than that of natural stellerite, accompanied with increasing specific surface area. On the contrary, NaOH modification induced the loss of photocatalytic ability of composite due to the generation of silicates.

1. Introduction

In recent years, with the rapid development of China's economy, the industry has achieved a rapid development. However, the environmental impact should not be overlooked. For example, the amount of discharge of papermaking wastewater amounted to 2.855 billion tons in 2013, accounting for 14.9% of total industrial wastewater.

The traditional industrial wastewater treatment included physical chemistry and biochemical methods [1, 2]. However, the adsorbable organic halogens (AOX) in wastewater cannot be effectively treated by those methods. It was reported that AOX can be decomposed by enzyme treatment, but the technique is still at the experimental stage because of high costs, considerable treatment time, and lack of substrates [3].

In recent years, titanium dioxide catalyst is generally applied for treating wastewater containing organic contaminants due to its excellent ability to achieve complete mineralization of the organic contaminants under moderate

conditions such as ambient temperature and ambient pressure [4, 5]. TiO₂ photocatalytic degradation of a cellulose ECF effluent was evaluated by Pérez et al. [6]. It was found that after 30 min of reaction more than 60% of the toxicity was removed and after 420 min of reaction none of the initial chlorinated low molecular weight compounds were detected, suggesting an extensive mineralization which was corroborated by 95 and 50% AOX and TOC removals, respectively.

However, the difficulties of the nano TiO₂ particle's fixation and recovery due to its small diameter seriously impede its industrialization, so the supported problem has become a hot research topic in TiO₂ photocatalysis domain at present.

Recent research has investigated many kinds of supports for dispersing TiO₂; zeolite [7], glass [8], stainless steel [9], carbon nanotube [10], and graphene [11] are some very recent examples reported in the literature.

Among these materials, zeolites are attractive candidates due to their uniform pores and channel sizes, huge surface area, high adsorption capacity, and low cost. However, the adsorption ability of natural zeolite to pollutants is very limited because the channels and cavities of the zeolite structure were blocked. In order to improve the absorption and exchange capacities and pollution treatment capabilities of zeolite, many attempts have been made such as ion exchange, organic modification, and calcination modification. Among them, the ion exchange modification method becomes the research focus because of its convenient operation, pollution, and environmental friendliness.

In this study, we are concerned with the photocatalytic decomposition of methyl orange (MO) over TiO_2 composite nanophotocatalyst prepared by dispersing TiO_2 on the surface of modified stellerite. The structure, crystal phase, morphology, BET surface area, and photocatalytic activity of the prepared photocatalyst were also investigated.

2. Experimental

2.1. Materials

2.1.1. Modified of Stellerite. Stellerite was obtained from Jinshansida Co. Ltd. (Guangxi, China). Chemical composition of the zeolite is $(\text{K}_{0.017}\text{Na}_{0.042}\text{Ca}_{1.13})_{1.189}[\text{Al}_{1.997}\text{Si}_{7.05}\text{O}_{18}] \cdot 6.75\text{H}_2\text{O}$. The stellerite was washed repeatedly by distilled water in order to remove some impurity ions and then was dehydrated in an oven box at 100°C for 12 h. 7.5 g of stellerite was put into a round flask containing 75 mL different concentrations of HCl, NaOH, or NaCl aqueous solution. The reaction was maintained at 90°C for 4 h under stirring. The solid-liquid mixture was filtrated afterwards, and the stellerite was cleaned with distilled water. A AgNO_3 test was performed to make sure that no Cl^- remained in the stellerite. After grinding, the stellerite was calcinated at 100°C for 12 h. These stellerites were denoted as $n\text{AcMS}$, $n\text{AlMS}$, and $n\text{SMS}$, where n is the concentration of HCl, NaOH, and NaCl aqueous solution.

2.1.2. Scanning Electron Microscopy (SEM) Analysis. Morphologies of the fracture surfaces were examined with a scanning electron microscope (SEM S3700, Hitachi, Japan) operating at an accelerating voltage of 10 kV. Before observation, the samples were coated with gold using a vacuum sputter-coater.

2.1.3. Fourier Transform Infrared Spectroscopy Analysis. Fourier transform infrared spectroscopy analysis (FTIR) of the samples was carried out in transmission mode using macro techniques (13 mm Φ pellet; *ca.* 1.5 mg sample with 350 mg KBr). The spectra were recorded with a Nexus Vector spectrometer made by Thermo Nicolet (Nexus 670, Thermo Nicolet Company, USA) under the following specifications: apodization: triangular; detector: DTGS/KBr; regulation: 4 cm^{-1} ; number of scans: 32.

2.1.4. X-Ray Diffraction Analysis. The X-ray powder diffraction patterns of the samples were recorded on Bruker D8

Advance X-ray diffractometer (step size 0.02°, 17.7 s per step). A generator with 40 kV and current of 40 mA was employed as a source for $\text{CuK}\alpha$ radiation.

2.1.5. Preparation of Photocatalyst. TiO_2 loaded on stellerite was prepared by sol-gel process. The precursor solution composites consist of tetra-n-butyl titanate, pure ethanol, and nitric acid. The nitric acid was used as catalyst to control the hydrolysis process. The detailed steps are as follows: A given amount of tetrabutyl titanate was dissolved in pure ethanol with a volume ratio of 1:4 of tetrabutyl titanate to ethanol, and then nitric acid solution was added dropwise into the solution to readjust the pH value to 4. Stirring for 20 min, a certain amount of natural stellerite or modified stellerite was added and the ratio of TiO_2 : stellerite is 28 : 100. Stirring for 10 min, a certain amount of distilled water was added and the volume ratio of distilled water : nitric acid is 1:1. After stirring for 15 min, weak gray sol was obtained and then dried at 100°C for 24 h and at 200°C for 4 h and ground to fine powder in an agate mortar. By this procedure, TiO_2 loaded on stellerite was prepared, denoted as $\text{TiO}_2/\text{stellerite}$ or $n\text{TiO}_2/\text{AcMS}$, $n\text{TiO}_2/\text{AlMS}$, and $n\text{TiO}_2/\text{SMS}$, where n is the concentration of HCl, NaOH, or NaCl aqueous solution in the procedure of stellerite modified treatment.

2.1.6. Characterization of Photocatalyst. The effect of stellerite modification on the photocatalytic activity of $\text{TiO}_2/\text{stellerite}$ photocatalyst was investigated using methyl orange (MO) as the target compound. A total amount of 0.8 g of photocatalyst was suspended in a 400 mL of 15 mg/L MO solution. The suspension was stirred magnetically for 30 min to reach adsorption equilibrium. The photocatalytic reactions were carried out in a quartz tube irradiated by 365 nm UV light (light irradiation of 2200 $\mu\text{W}/\text{cm}^2$). The suspensions were withdrawn at intervals and centrifuged at 14,000 rpm for 10 min and then the residual concentration of MO was determined in solution at 460 nm using a UV-Vis spectrophotometer (DR5000, HACH, USA). The removal rate of MO was calculated by the following equation:

$$\eta = \frac{C_0 - C}{C_0} = \frac{A_0 - A}{A_0} \times 100\%, \quad (1)$$

where C_0 and A_0 are the initial concentration and absorbency of MO solution; C and A are the concentration and absorbency of MO solution after a certain time. Control experiments (direct photolysis) were also carried out without the addition of photocatalyst.

All experiments were run in triplicate with the relative standard deviations (RSD) of about 5%.

3. Results and Discussion

3.1. SEM Imaging of Natural and Modified Stellerites. The surface morphology of natural and modified stellerites is shown in Figure 1. It was found that natural stellerite occurs as clear layer shape structure. As a result of HCl and NaCl modification, microcracks developed on the surface of stellerite. However, the layer shape structure of stellerite changes

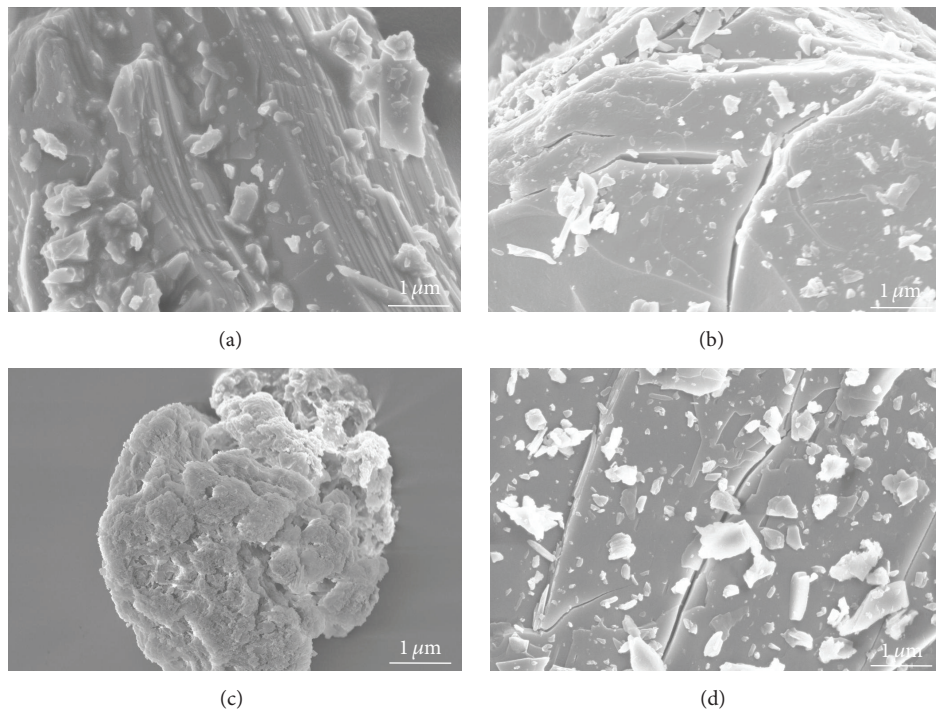


FIGURE 1: SEM images of natural and modified stellerites: (a) natural stellerite, (b) 1.0AcMS, (c) 0.2AlMS, and (d) 1.0SMS.

to irregular granular structure because of the corrosion by NaOH solution.

3.2. Si/Al Atomic Ratio. The influence on the Si/Al atomic ratios of stellerites by different concentrations of modifying agents is shown in Figure 2. In HCl modification, the Si/Al atomic ratio was raised with the increase of HCl concentration and 13.86 (surged almost fourfold) of Si/Al atomic ratio was obtained by HCl modification with the concentration of 1.0 mol/L, indicating that HCl has a strong dealuminization power correlated with the occurrence of hydroxy nests [12]. The dealuminization reaction can be represented as in Scheme 1.

Instead, the Si/Al atomic ratio decreased with the increase in the concentration of NaOH and NaCl, particularly in NaOH modification; these results are in accord with previous report [13]. The mechanism of silica dissolution is shown in Scheme 2.

3.3. FTIR Spectra Analysis. The FTIR spectra of natural and modified stellerite samples are shown in Figure 3. The bands at 3480 and 1642 cm^{-1} were attributed to the valence and bending vibrations of water molecules in stellerite. The peak at 1040 cm^{-1} indicates the asymmetrical extensional vibrations of Si(Al)-O. The bands at 795 and 456 cm^{-1} were due to the symmetric stretching and bending vibrations of Si(Al)-O.

An obvious shift of the IR vibrations to high frequency for 1.0AcMS in comparison with that of the corresponding natural stellerite sample indicates the dealumination during

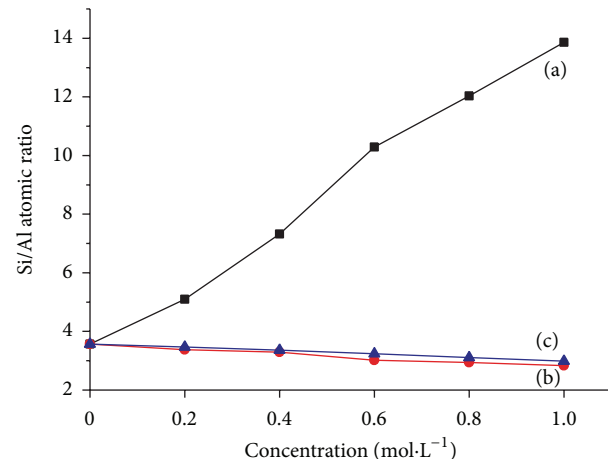
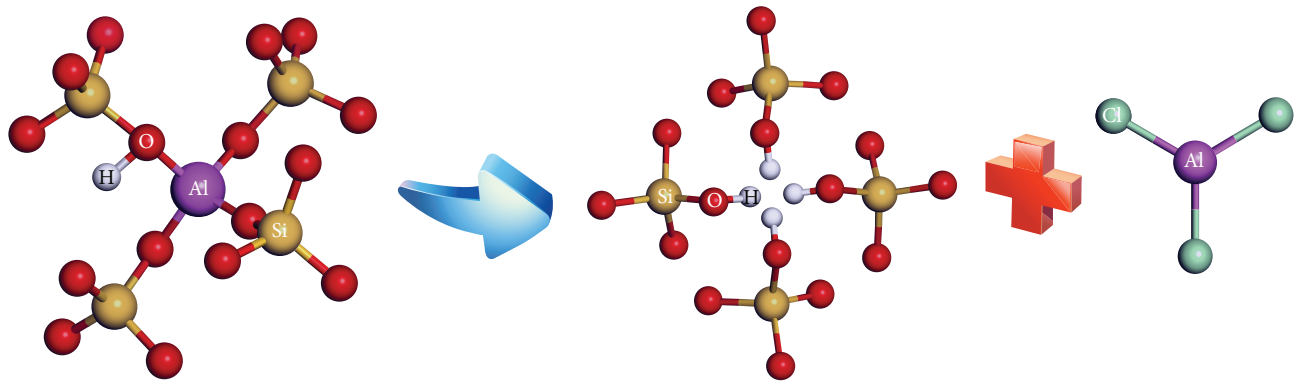
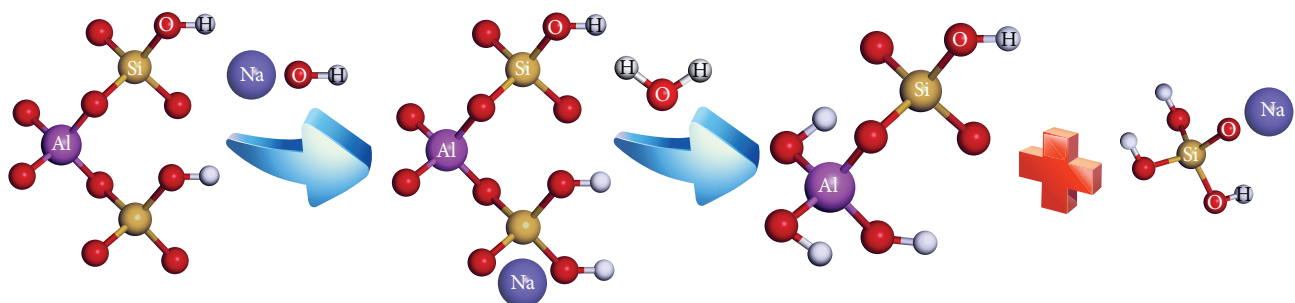


FIGURE 2: Si/Al atomic ratios of natural and modified stellerites: (a) HCl modification, (b) NaOH modification, and (c) NaCl modification.

hydrochloric acid modification. The blue shift is particularly obvious for the Si(Al)-O intensive asymmetric stretching vibrations at about 1040 cm^{-1} . By contrast, NaOH modification caused noticeable red shift at 1035 cm^{-1} in spectra (c) because of the desilication processes (the vibration frequency of Si-O is higher than Al-O). Contrary to the spectra of (a) and (d), most band positions did not change following NaCl modification, suggesting that the base stellerite did not collapse.



SCHEME 1: Schematic representation of the dealumination upon treatment in hydrochloric acid.



SCHEME 2: Schematic representation of the desilication upon treatment in NaOH solution.

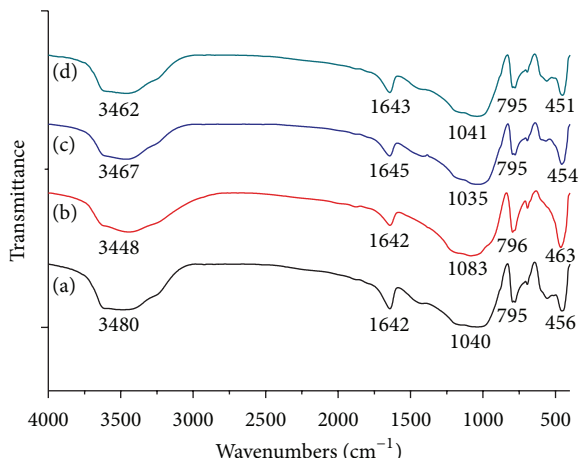


FIGURE 3: FTIR spectra of (a) natural stellerite, (b) 1.0AcMS, (c) 0.2AlMS, and (d) 1.0SMS.

3.4. Structural Analysis. Table 1 presents the parameters of porous structure of various samples. The S_{BET} value for natural stellerite is $2.2 \text{ m}^2/\text{g}$; in the case of treatment of stellerite with 0.4 M HCl , its S_{BET} value grows to $67.9 \text{ m}^2/\text{g}$ and the V_{BET} value grew by 7 times. Besides, D_{BET} and D_{BJH} of the HCl and NaCl modified samples are also significantly smaller in comparison with the natural stellerite, indicating the creation of microporous structure. However, D_{BET} and D_{BJH} of the NaOH modified sample grow to 12.7 and 41.0 nm

and reveal that NaOH modified stellerite can bring about different effect of surface topography compared with HCl and NaCl modified stellerite, and this result is consistent with Figure 1.

The adsorption-desorption isotherms for natural and modified stellerite are shown in Figure 4. Based on conventional classification of adsorption, the isotherms of natural and 0.2AlMS can be considered as isotherms of IV type with the hysteresis loop of the type H3. In comparison, the nitrogen adsorption on the HCl and NaCl modified stellerite is expressed by I type isotherm with wide hysteresis loop which does not close at low relative pressure. The obvious increases of the micropore volumes of the HCl and NaCl modified stellerite are caused by unblocking of the channels of framework structure of stellerite through dealumination during acid modification or ion exchange action during NaCl modification.

3.5. X-Ray Diffraction Analysis. X-ray examination of the different samples showed (Figure 5) that modifications of stellerite did not damage the stellerite structure that is characterized by the main peaks at 2θ equal to 9.759° which can be assigned as $\{020\}$. The characteristic XRD peaks of anatase were observed at $2\theta = 25.352^\circ$, 37.784° , 48.072° , 53.928° , and 55.115° for TiO_2 supported on modified stellerite, which can be assigned as $\{101\}$, $\{004\}$, $\{200\}$, $\{105\}$, and $\{221\}$. No significant rutile peak was found, showing that rutile phase did not form on the surface of stellerite.

TABLE 1: The parameters of stellerite porous structures by nitrogen adsorption/desorption method.

| Sample | Specific surface area (m^2/g) | | | Pore volume (cm^3/g) | | Pore size (nm) | |
|---------|-------------------------------------------------|-------|-------|----------------------------------------|------------------|------------------|------------------|
| | S_{BET} | S_m | S_e | V_{BET} | V_{BJH} | D_{BET} | D_{BJH} |
| Natural | 2.2 | 1.1 | 1.1 | 0.0045 | 0.0096 | 8.2 | 38.7 |
| 0.4AcMS | 67.9 | 53.7 | 14.2 | 0.0363 | 0.0088 | 2.1 | 10.2 |
| 0.2AlMS | 18.0 | 1.5 | 16.5 | 0.0570 | 0.1244 | 12.7 | 41.0 |
| 1.0SMS | 33.1 | 23.9 | 9.2 | 0.0216 | 0.0154 | 2.6 | 10.4 |

$S_m = S_{\text{t-plot}}$ (micropore area); $S_e = S_{\text{t-plot}}$ (external surface area).

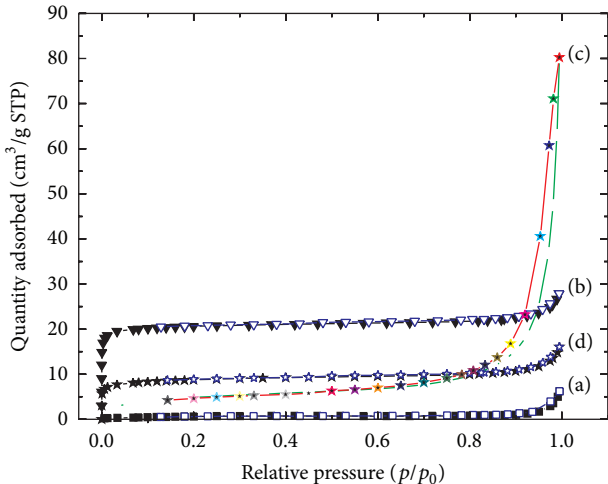


FIGURE 4: Low temperature of adsorption/desorption isotherms of nitrogen on different samples: (a) natural stellerite, (b) 0.4AcMS, (c) 0.2AlMS, and (d) 1.0SMS.

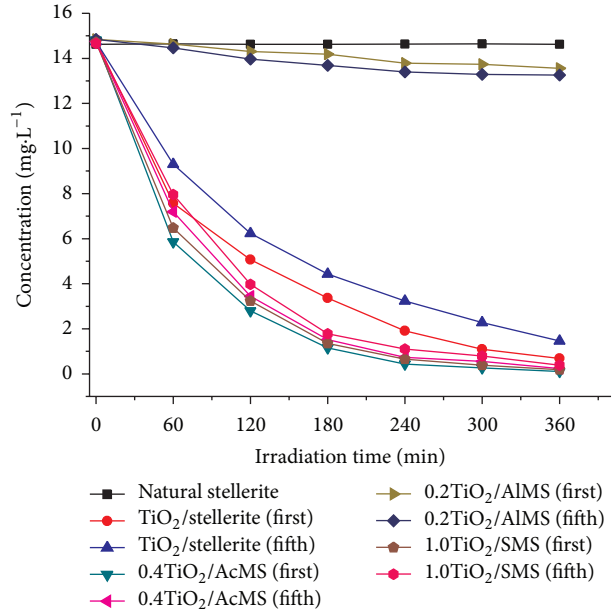


FIGURE 6: MO photocatalytic degradation with prolonged irradiation time.

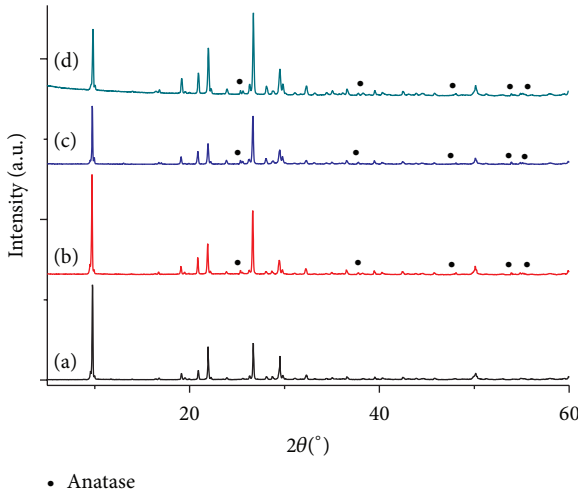


FIGURE 5: XRD patterns of (a) natural stellerite, (b) 0.4TiO₂/AcMS, (c) 0.2TiO₂/AlMS, and (d) 1.0TiO₂/SMS. The ratio of TiO₂ : modified stellerite was fixed to 28:100.

3.6. Photocatalytic Activity. Figure 6 shows the relationship between MO degradation and irradiation time for different TiO₂ loaded samples at 2 g/L of photocatalyst. Photocatalytic activity of natural stellerite was also studied as comparison. It was found that natural stellerite has no photocatalytic

activity on MO degradation under UV irradiation. MO degradation rates increased with irradiation time using either TiO₂/stellerite or TiO₂ load modified stellerite. After 180 min of irradiation, MO degradation rates were 77.60%, 92.33%, and 91.00% using TiO₂/stellerite, 0.4TiO₂/AcMS, and 1.0TiO₂/SMS as photocatalyst. The results show that photocatalytic activity of TiO₂ is improved by HCl and NaCl modification of stellerite. The photocatalyst was recycled after filtration and heating treatment at 100°C for 12 h and 200°C for 2 h in every cycle. After four cycles, MO orange degradation rates decreased from 77.60%, 92.33%, and 91.00% to 70.47%, 89.86%, and 88.13%, respectively. The slight decrease of photocatalytic activity was due to TiO₂ loss from the surface of stellerite and the fouling of the photocatalyst by byproducts during degradation.

On the contrary, the photocatalytic activity of 0.2TiO₂/AlMS was also disappeared due to the follow reasons: First, the porous structure of stellerite was damaged to some extent by NaOH; second, the photocatalysts agglomerate together to form larger clusters due to the viscous silicates; third, the transparency of the solution was decreased by silicates.

4. Conclusions

- (1) TiO_2 was dispersed using sol-gel method on the surfaces of stellerite treated by HCl, NaOH, or NaCl.
- (2) The S_{BET} value of stellerite was increased by modification. D_{BET} of natural stellerite, 0.4AcMS, 0.2AlMS, and 1.0SMS was 8.2, 2.1, 12.7, and 2.6 nm, respectively. HCl and NaCl modification stimulate the production of micropores, and the surface of stellerite appeared to dissolve by NaOH modification.
- (3) The photocatalytic activity of 0.4 TiO_2 /AcMS and 1.0 TiO_2 /SMS was better than that of natural stellerite. The composite photocatalyst had excellent photocatalytic activity after four recycles.

Conflict of Interests

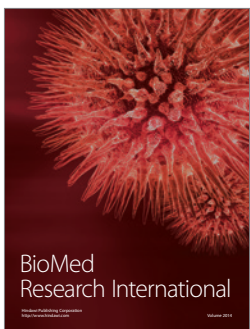
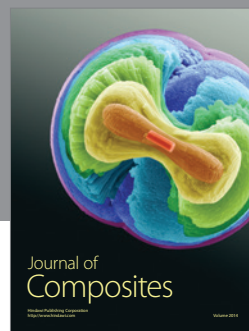
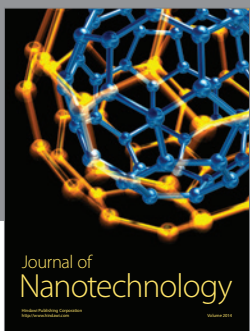
The authors declare that there is no conflict of interests regarding the publication of this paper.

Acknowledgments

The authors would like to acknowledge support from the Key Projects in the National Science & Technology Pillar Program during the Twelfth Five-year Plan Period (Grant no. 2013BAC16B04).

References

- [1] Y. Tian, H. Li, L. P. Li et al., "In-situ integration of microbial fuel cell with hollow-fiber membrane bioreactor for wastewater treatment and membrane fouling mitigation," *Biosensors & Bioelectronics*, vol. 64, pp. 189–195, 2015.
- [2] A. G. D. Prasad and M. A. Abdullah, "Biosorption of Cr(VI) from synthetic wastewater using the fruit shell of gulmohar (*delonix regia*): application to electroplating wastewater," *BioResources*, vol. 5, no. 2, pp. 838–853, 2010.
- [3] D. Pokhrel and T. Viraraghavan, "Treatment of pulp and paper mill wastewater—a review," *Science of the Total Environment*, vol. 333, no. 1–3, pp. 37–58, 2004.
- [4] Ö. Kerkez and İ. Boz, "Photodegradation of methylene blue with $\text{Ag}_2\text{O}/\text{TiO}_2$ under visible light: operational parameters," *Chemical Engineering Communications*, vol. 202, no. 4, pp. 534–541, 2015.
- [5] N. Mahmoud, T. Ahmed, O. Shinichi, and S. Masaaki, "Biological hydrogen production from starch wastewater using a novel up-flow anaerobic staged reactor," *BioResources*, vol. 8, no. 4, pp. 4951–4968, 2013.
- [6] M. Pérez, F. Torrades, J. Peral et al., "Multivariate approach to photocatalytic degradation of a cellulose bleaching effluent," *Applied Catalysis B: Environmental*, vol. 33, no. 2, pp. 89–96, 2001.
- [7] L. Chen and B. Yan, "Multi-color luminescence of hybrids based with lanthanide functionalized zeolite A and titania," *Colloid and Polymer Science*, vol. 293, no. 6, pp. 1847–1853, 2015.
- [8] M. R. Espino-Estévez, C. Fernández-Rodríguez, O. M. González-Díaz, J. A. Navío, D. Fernández-Hevia, and J. M. Doña-Rodríguez, "Enhancement of stability and photoactivity of TiO_2 coatings on annular glass reactors to remove emerging pollutants from waters," *Chemical Engineering Journal*, vol. 279, pp. 488–497, 2015.
- [9] D. C. L. Vasconcelos, E. H. M. Nunes, A. C. S. Sabioni, P. M. P. Vasconcelos, and W. L. Vasconcelos, "Optical characterization of 316L stainless steel coated with sol-gel titania," *Journal of Non-Crystalline Solids*, vol. 358, no. 22, pp. 3042–3047, 2012.
- [10] Z. H. Gao, Z. D. Cui, S. L. Zhu, Y. Q. Liang, Z. Y. Li, and X. J. Yang, "Design and synthesis of MWNTs- TiO_2 nanotube hybrid electrode and its supercapacitance performance," *Journal of Power Sources*, vol. 283, pp. 397–407, 2015.
- [11] A. J. Wang, W. Yu, Y. Fang et al., "Facile hydrothermal synthesis and optical limiting properties of TiO_2 -reduced graphene oxide nanocomposites," *Carbon*, vol. 89, pp. 130–141, 2012.
- [12] M.-C. Silaghi, C. Chizallet, and P. Raybaud, "Challenges on molecular aspects of dealumination and desilication of zeolites," *Microporous and Mesoporous Materials*, vol. 191, pp. 82–96, 2014.
- [13] Z. Liang and J. R. Ni, "Improving the ammonium ion uptake onto natural zeolite by using an integrated modification process," *Journal of Hazardous Materials*, vol. 166, no. 1, pp. 52–60, 2009.




Hindawi

Submit your manuscripts at
<http://www.hindawi.com>

